

Evolution of superconductivity and charge order in pressurized RbV_3Sb_5

Feng Du,^{1,2} Shuaishuai Luo,^{1,2} Rui Li,^{1,2} Brenden R. Ortiz,³ Ye Chen,^{1,2} Stephen D. Wilson,³ Yu Song,^{1,2,*} and Huiqiu Yuan^{1,2,4,†}

¹Center for Correlated Matter and Department of Physics, Zhejiang University, Hangzhou 310058, China

²Zhejiang Province Key Laboratory of Quantum Technology and Device,
Department of Physics, Zhejiang University, Hangzhou 310058, China

³Materials Department and California Nanosystems Institute,
University of California Santa Barbara, Santa Barbara, CA, 93106, United States

⁴State Key Laboratory of Silicon Materials, Zhejiang University, Hangzhou 310058, China

The kagome metals AV_3Sb_5 ($A = \text{K}, \text{Rb}, \text{Cs}$) under ambient pressure exhibit an unusual charge order, from which superconductivity emerges. In this work, by applying hydrostatic pressure using a liquid pressure medium and carrying out electrical resistance measurements for RbV_3Sb_5 , we find the charge order becomes suppressed under a modest pressure p_c ($1.4 < p_c < 1.6$ GPa), while the superconducting transition temperature T_c is maximized. T_c is then gradually weakened with further increase of pressure and reaches a minimum around 14.3 GPa, before exhibiting another maximum around 22.8 GPa, signifying the presence of a second superconducting dome. Distinct normal state resistance anomalies are found to be associated with the second superconducting dome, similar to KV_3Sb_5 . Our findings point to qualitatively similar temperature-pressure phase diagrams in KV_3Sb_5 and RbV_3Sb_5 , and suggest a close link between the second superconducting dome and the high-pressure resistance anomalies.

I. INTRODUCTION

The kagome metals AV_3Sb_5 ($A = \text{K}, \text{Rb}, \text{Cs}$) [1–4] have drawn significant interest recently, with focus on (1) superconductivity with topological surface states [2], which raises the prospects of realizing topological superconductivity and Majorana zero modes [5, 6]; (2) a large anomalous Hall effect in the absence of local moments [7–9], which possibly results from a charge order that breaks time-reversal symmetry [10–13]; (3) the nature of the superconducting pairing, with evidence for nodeless superconducting gaps [14–16], as well as indications for nematic superconductivity [17]; and (4) the sensitivity of superconductivity and charge order to pressure-tuning [18–26], likely related to the presence of competing instabilities on the kagome lattice [27–31].

With the application of pressure, the charge order becomes quickly suppressed and superconductivity is enhanced, forming a superconducting dome with maximal T_c near the pressure at which charge order disappears [18–24, 26]. While this superconducting dome can be understood to result from the competition between superconductivity and charge order, a second superconducting dome is found in AV_3Sb_5 at higher pressures [18, 21–24], whose origin remains unclear. Factors that may be relevant for the formation of the second superconducting dome include a pressure-induced Lifshitz transition [22], magnetism suppressing superconductivity in the region between the two superconducting domes [32], reconstruction of the Sb bands due to the formation of interlayer Sb-Sb bonds [33], and a distinct high-pressure phase revealed through resistivity anomalies [21]. While two-dome superconductivity is found in all AV_3Sb_5 materials via resistivity measurements [24], studies of the corresponding normal state from which superconductivity emerges has been limited [21, 22]. In particular, it remains unclear whether resistivity anomalies associated with the second superconducting dome in KV_3Sb_5 [21] are also present in RbV_3Sb_5 and CsV_3Sb_5 .

In addition, single crystal diffraction revealed a highly anisotropic compression under hydrostatic pressure, with the c lattice parameter reducing significantly more than the in-plane lattice parameters [33], which suggests hydrostaticity of measurements under pressure may strongly affect experimental results and the determined phase diagrams. Therefore, to compare results on the AV_3Sb_5 series obtained using different experimental techniques, it is important to reproduce the corresponding experimental hydrostaticity.

In this work, we systematically investigated the temperature-pressure phase diagram of RbV_3Sb_5 via measurements of electrical resistance, applying pressure using a liquid pressure medium. It is found that the superconducting transition temperature T_c in RbV_3Sb_5 increases from 0.9 K under ambient pressure to about 4.5 K at 1.2 GPa, with the charge order disappearing above p_c , which occurs between 1.4 and 1.6 GPa. T_c is then gradually suppressed with increasing pressure and reaches a minimum of about 0.4 K around 14.3 GPa. With further increase of pressure, another T_c maximum of about 1.2 K is observed around 22.8 GPa, indicating the presence of a second superconducting dome. For pressures $\gtrsim 22.8$ GPa, T_c in the second superconducting dome is suppressed with increasing pressure, and distinct features are detected in the normal state resistance, possibly related to a high-pressure phase. These behaviors are similar to pressurized KV_3Sb_5 [21], suggesting that they are common in the AV_3Sb_5 series under high pressure,

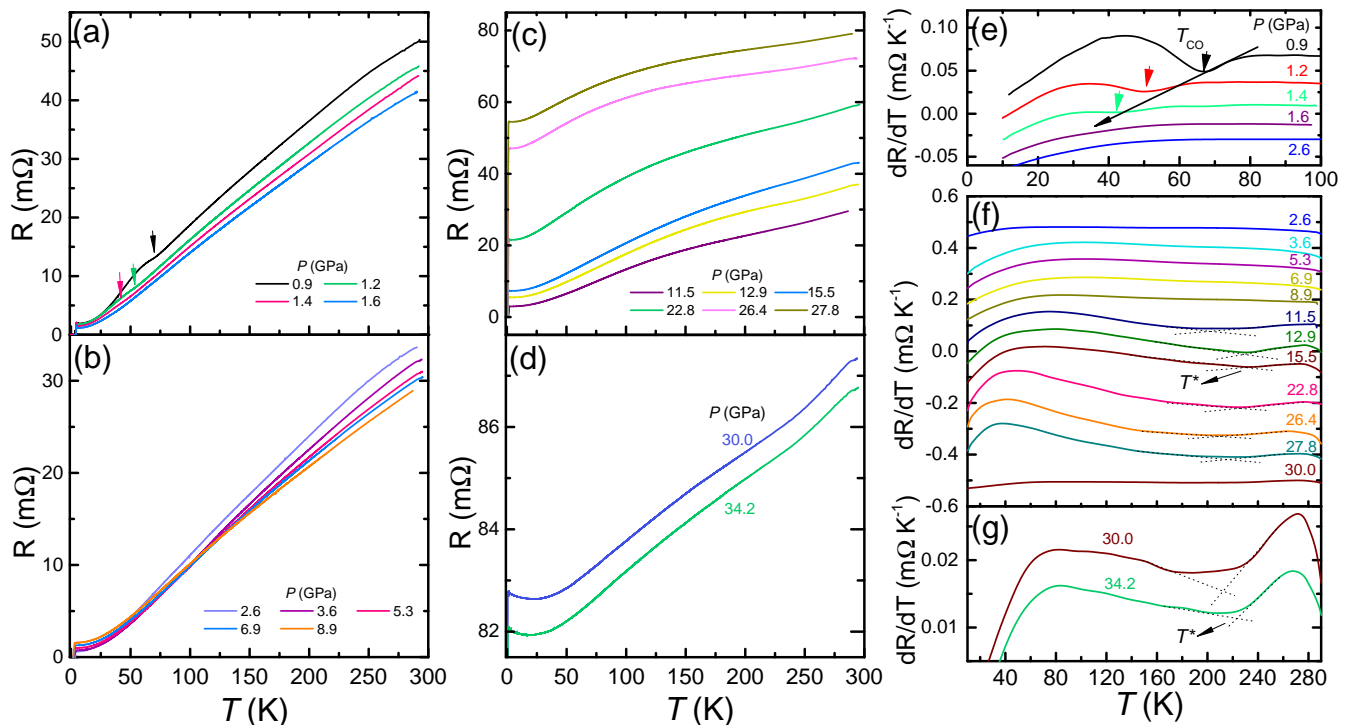


Figure 1: (a)-(d): Electrical resistance $R(T)$ of RbV₃Sb₅ sample #1 in various pressure ranges. (e)-(g): The corresponding dR/dT curves, shifted vertically for clarity. T_{CO} is the onset temperature of the charge order, and T^* corresponds to a minimum in dR/dT .

and are closely related to the suppression of superconductivity in the second dome.

II. EXPERIMENTAL DETAILS

Single crystals of RbV₃Sb₅ were grown using a self-flux method [1, 2]. Electrical resistance measurements under pressure were carried out using a diamond anvil cell (DAC), with silicon oil as the pressure medium, which allows for better hydrostaticity compared to solid pressure media. Single crystals of RbV₃Sb₅ were polished and cut into square pieces, and then loaded into a Be-Cu diamond anvil cell with a 400- μ m-diameter culet. The ruby fluorescence method was used to determine the values of pressure inside the DAC at room temperature, before and after the measurements. All electrical resistance measurements from room temperature down to 0.3 K were performed in a Teslatron-PT system with an Oxford ³He insert. For measurements with an applied magnetic field, the field was applied along the c -axis.

III. RESULTS

Measurements of the electrical resistance $R(T)$ for sample #1 with pressures from 0.9 GPa up to 34.2 GPa are shown in Figs. 1(a)-(d), with the corresponding dR/dT curves shown in Figs. 1(e)-(g). Examining the behavior of $R(T)$ in the normal state, clear anomalies associated with the charge ordering temperature T_{CO} can be seen up to 1.4 GPa, with T_{CO} decreasing with increasing pressure [Fig. 1(a)]. The values of T_{CO} can be determined from the anomaly in the dR/dT curves, as shown in Fig. 1(e), which becomes indiscernible at 1.6 GPa. These results suggest the charge order disappears at a critical pressure p_c between 1.4 and 1.6 GPa. p_c in RbV₃Sb₅ is larger than that in KV₃Sb₅ (\approx 0.5 GPa) [21], consistent with the idea that larger alkaline metal ions exert negative chemical pressure, although it should be noted that additional effects may also be at play, as suggested by the complex evolution of T_c with pressure in CsV₃Sb₅ and RbV₃Sb₅ for $p < p_c$ [19, 20, 26].

In the pressure range 2.6 GPa to 8.9 GPa, $R(T)$ in the normal state is largely unchanged with increasing pressure [Fig. 1(b)]. In contrast, in the pressure range 11.5 GPa to 27.8 GPa, the values of $R(T)$ increase with increasing

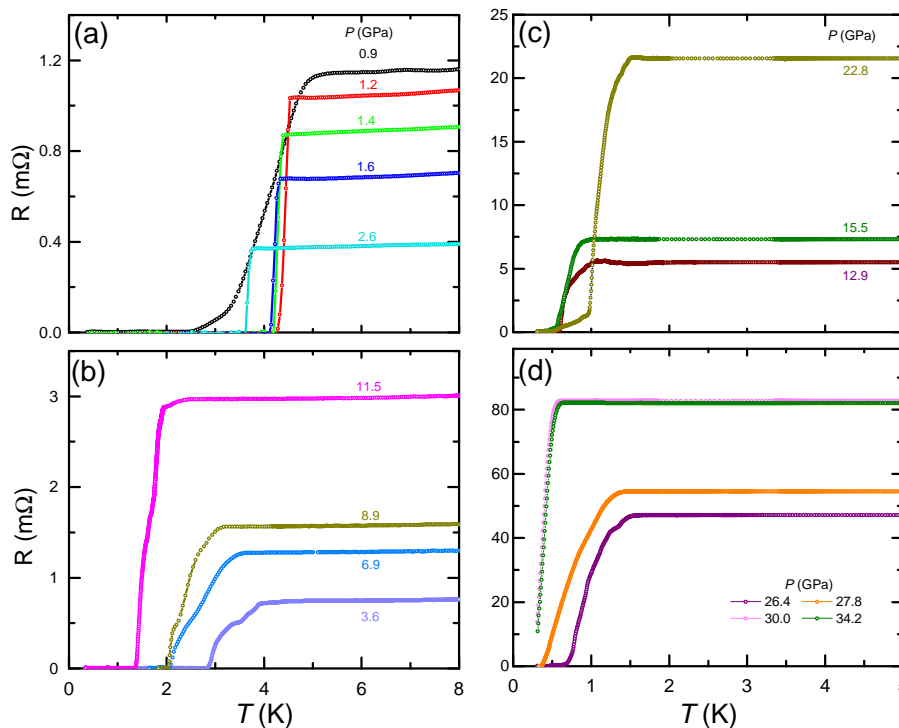


Figure 2: Zoomed-in electrical resistance $R(T)$ of RbV₃Sb₅ sample #1 under various pressures to show the evolution of superconductivity with pressure.

pressure, with the increase particularly prominent for $p \gtrsim 22.8$ GPa [Fig. 1(c)]. This difference between the results in Figs. 1(b) and (c) is largely due to the residual resistance R_0 , which is the value of $R(T)$ just before the onset of superconductivity. On the other hand, the variation of $R(T)$ with temperature, which can be captured by $\delta R = R(300 \text{ K}) - R_0$, stays nearly unchanged from 2.6 GPa to 22.8 GPa, but starts to decrease dramatically when $p \gtrsim 22.8$ GPa. Clear anomalies in dR/dT , with a minimum at $T^* \sim 220$ K [Figs. 1(f) and (g)], are detected for $p \gtrsim 11.5$ GPa. It should be noted that since dR/dT exhibits multiple anomalies around T^* , with possible additional features above room temperature, T^* should be considered as a characteristic temperature rather than a transition temperature.

For even higher pressures of 30.0 GPa and 34.2 GPa, the normal state $R(T)$ becomes qualitatively different: compared to lower pressures, the values of δR are much smaller, R_0 becomes much larger [Fig. 1(d)], and a subtle upturn in $R(T)$ is observed for $T \lesssim 20$ K. In addition, the dR/dT anomaly associated with T^* becomes more dominant for $p \gtrsim 30.0$ GPa, due to the dramatic decrease of δR (and thus the magnitude of dR/dT) at these pressures. These behaviors are similar to KV₃Sb₅ at high pressures [21], and can be collectively attributed to the formation of a high-pressure phase.

Since the high-pressure phase exhibits a small δR and a large R_0 , the observation that δR begins to drop while R_0 begins to increase for $p \gtrsim 22.8$ GPa suggests that the high-pressure phase onsets around 22.8 GPa. On the other hand, signatures of T^* already appears for 11.5 GPa, a significantly lower pressure compared to when δR begins to drop and R_0 begins to increase, suggesting that is not unique to the high-pressure phase. More work is needed to definitively pin down the phase boundary of the high-pressure phase in the temperature-pressure phase diagram and elucidate the origin of the resistance anomalies around T^* .

Fig. 2 zooms into low temperatures to examine the evolution of superconductivity in RbV₃Sb₅ sample #1, as a function of applied pressure. For pressures from 0.9 GPa to 2.6 GPa [Fig. 2(a)], T_c is bunched around 4 K, significantly higher than $T_c < 1$ K under ambient pressure [3]. A prominent feature is that the superconducting transition is significantly broader for 0.9 GPa, compared to those from 1.2 to 2.6 GPa, which suggests that a broad superconducting transition is correlated with the presence of a strong charge order. It should be noted that while signatures of the charge order is also detected for 1.2 GPa and 1.4 GPa, the corresponding dip in dR/dT is significantly weakened compared to 0.9 GPa, which indicates that the magnitude of the charge order parameter becomes significantly reduced. A similar sharpening of the superconducting transition with weakening of the charge order upon applying pressure is

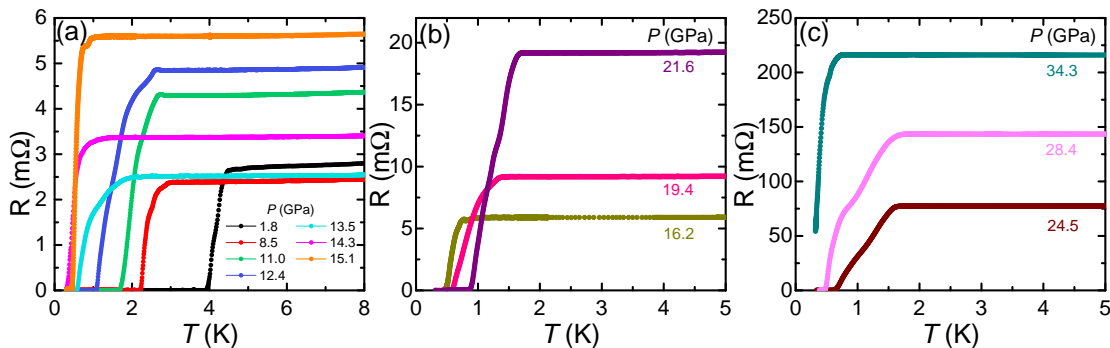


Figure 3: Electrical resistance $R(T)$ of RbV₃Sb₅ sample #2 near the superconducting transition under various pressures, showing the evolution of superconductivity with pressure.

also observed in KV₃Sb₅ [21], suggesting that it is a common feature of the AV₃Sb₅ series.

One possible origin for this behavior is that dT_c/dp is much larger in the presence of a strong charge order, compared to when the charge order is significantly weakened or suppressed. If there is a distribution of internal stress Δp in the sample (and assume that it does not change too much with applied pressure), then the superconducting transition width $\Delta T_c \approx \frac{dT_c}{dp} \Delta p$, would be large when dT_c/dp is large.

Alternatively, domain boundaries of a period-2 charge order could exhibit enhanced filamentary superconductivity, leading to a broad superconducting transition in $R(T)$. Such a picture was invoked to account for enhanced superconductivity seen in the period-2 charge order phase of Ba_{1-x}Sr_xNi₂As₂, while such an effect is absent for the period-3 charge order phase in the same material series [34]. Given the charge order in AV₃Sb₅ is period-2 in the ab -plane [2], such a mechanism may also contribute to its broadened superconducting transition under ambient and low pressures, where the charge order is substantial.

In the pressure range 3.6 GPa to 11.5 GPa [Fig. 2(b)], T_c gradually reduces with increasing pressure, which in combination with results in Fig. 2(a), evidence a superconducting dome with maximal T_c around p_c . Such a behavior was previously reported for the AV₃Sb₅ materials [18–21, 24], and likely results from a competition between charge order and superconductivity, without a prominent role of quantum criticality [21].

Upon further increasing pressure, T_c further drops for 12.9 GPa and 15.5 GPa, but becomes enhanced again at 22.8 GPa [Fig. 2(c)]. This suggests the presence of a minimum in T_c between 12.9 GPa and 22.8 GPa, and signifies the appearance of a second superconducting dome. For pressures in the range 26.4 GPa to 34.2 GPa [Fig. 2(d)], T_c decreases with increasing pressure, indicating that the maximal T_c of the second superconducting dome appears at $p < 26.4$ GPa. Moreover, the superconducting transition becomes sharpened for 30.0 and 34.2 GPa, possibly related to the high-pressure phase, with clear signatures in the normal state. It is interesting to note that the suppression of superconductivity in RbV₃Sb₅ is less significant compared to KV₃Sb₅, as the high-pressure phase appears. Compared to superconducting transitions for $p \leq 2.6$ GPa, those for $p \geq 3.6$ GPa are generally broader and less smooth, possibly related to a larger distribution of stress or pressure-induced defects in the crystal.

To clarify the evolution of T_c near the boundary of the two superconducting domes, we measured $R(T)$ near T_c for RbV₃Sb₅ sample #2, with results shown in Fig. 3. Upon increasing pressure from 1.8 GPa up to 14.3 GPa [Fig. 3(a)], T_c monotonically decreases with increasing pressure, with the value of T_c (determined through the midpoint of the superconducting transition) reaching a minimum of about 0.4 K at 14.3 GPa. With further increase of pressure, T_c becomes slightly enhanced at 15.1 GPa, and further increases with increasing pressure up to 21.6 GPa [Fig. 3]. Upon further increase of pressure, T_c again reduces with increasing pressure [Fig. 3]. These measurements on sample #2 are consistent with those for sample #1 [Fig. 2] in establishing the presence of two superconducting domes, and further clarifies that the minimum in T_c between the two domes occurs around 14.3 GPa.

To probe the superconducting state under various pressures, we chose three representative pressures and measured the resistance for sample #1 under an applied magnetic field along the c -axis, with results shown in Fig. 4. The three pressures correspond to states with coexisting charge order and superconductivity [0.9 GPa, Fig. 4(a)], without charge order and inside the first superconducting dome [2.6 GPa, Fig. 4(b)], and inside the second superconducting dome [27.8 GPa, Fig. 4(c)]. As can be seen, superconductivity is gradually suppressed with applied field in all cases, which allows us to extract the upper critical field $\mu_0 H_{c2}(T)$ for various pressures.

The upper critical fields $\mu_0 H_{c2}(T)$ are determined as when $R(T)$ drops to $R_0/2$, and are summarized in Fig. 4(d). $\mu_0 H_{c2}(T)$ could be fit with the Werthamer-Helfand-Hohenberg (WHH) model [35] for the three pressures, with fits

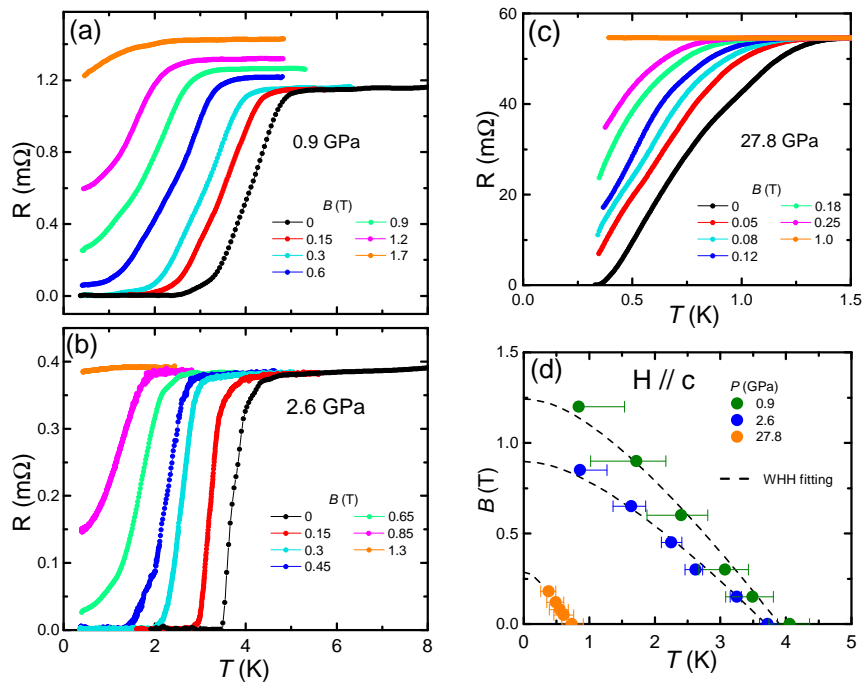


Figure 4: Low-temperature electrical resistance $R(T)$ of RbV₃Sb₅ sample #1 under various c -axis magnetic fields, for applied pressures (a) 0.9 GPa, (b) 2.6 GPa, and (c) 27.8 GPa. (d) The upper critical fields of RbV₃Sb₅, as a function of temperature under pressures of 0.9, 2.6, and 27.8 GPa. Fits to the WHH model are shown as dashed lines.

shown as dashed lines in Fig. 4(d). Previously, it was shown in KV₃Sb₅ that a much larger $\mu_0 H_{c2}(T=0)$ (for field along the c -axis) is observed for the second superconducting dome, even when the T_c is lower compared to the first superconducting dome [21]. For RbV₃Sb₅, the values of $T_c^2/\mu_0 H_{c2}(T=0)$ are respectively found to be 13.3, 15.2 and 1.9 (K²/T), for 0.9 GPa, 2.6 GPa and 27.8 GPa. The significantly smaller ratio at 27.8 GPa points to $\mu_0 H_{c2}(T=0)$ also becoming enhanced relative to T_c in the second superconducting dome, similar to KV₃Sb₅.

The phase diagram obtained from electrical resistance measurements under pressure is shown in Fig. 5(a). T_c is determined as when $R(T)$ drops to $R_0/2$, T^* from a minimum in dR/dT [Fig. 1(g)], and T_{CO} from the dip in dR/dT [Fig. 1(e)]. In KV₃Sb₅, it was shown that the decrease of T_c above p_c is much more gradual, compared to the enhancement of T_c below p_c , resulting in the first superconducting dome being highly asymmetric [21]. In the case of RbV₃Sb₅, it can be seen that the same qualitative behavior is observed.

Various regimes in the phase diagram can be identified through the presence of a resistivity anomaly at T^* [Fig. 5(a)] and signatures in δR and R_0 [Fig. 5(b)]. The anomaly in dR/dT associated with T^* first appears at 11.5 GPa, just before superconductivity crossovers from the first dome into the second. R_0 increases slowly with increasing pressure up to ≈ 22.8 GPa, above which it increases at a much faster rate up to ≈ 30 GPa, and finally plateaus for $p \gtrsim 30$ GPa. δR exhibits a gradual decrease with increasing pressure up to 1.4 GPa ($\approx p_c$), then evolves slowly up to ≈ 22.8 GPa, before dropping precipitously for $p \gtrsim 22.8$ GPa. Since T_c in the second superconducting dome begins to decrease with increasing pressure for $p \gtrsim 22.8$ GPa, a large R_0 and a small δR , which are signatures of a possible high-pressure phase, appear to be correlated with suppression of T_c in the second superconducting dome. A similar large drop of δR and an increase in R_0 are also observed in KV₃Sb₅, and are also associated with the suppression of T_c in the second superconducting dome [21].

IV. DISCUSSION AND CONCLUSION

Our observation of two-dome superconductivity is similar to previous works on AV₃Sb₅ [18, 21–24], and suggests that such a feature is qualitatively robust, both with regards to variation of the alkaline metal and experimental hydrostaticity. On the other hand, the additional modulation of T_c for $p < p_c$ in CsV₃Sb₅ and RbV₃Sb₅ [19, 20, 26] is not observed in KV₃Sb₅ [21]. While the present data on RbV₃Sb₅ suggests a single peak in T_c around p_c , the density of probed pressures is insufficient to distinguish whether additional subtle modulations of T_c exist for $p < p_c$ [26].

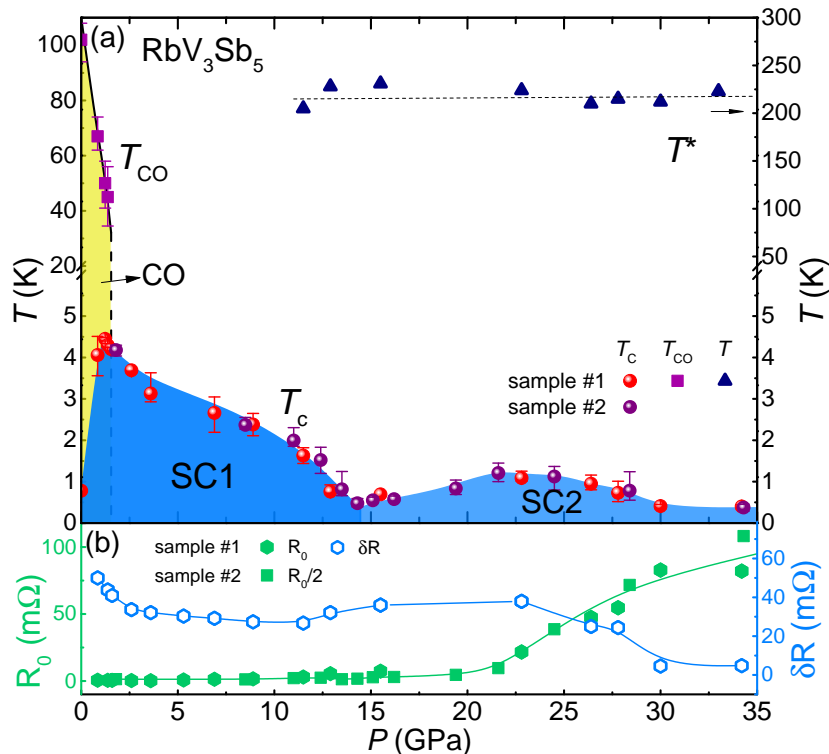


Figure 5: (a) The temperature-pressure phase diagram of RbV_3Sb_5 . Two superconducting regions (SC1 and SC2) and a charge-ordered phase (CO) are identified. Points under ambient pressure are from Ref. [3]. T_{CO} is the onset temperature of the charge order, T_c is the superconducting transition temperature, and T^* is a characteristic temperature associated with a minimum in dR/dT . The errors bars for T_{CO} are determined from the half width at half minimum of the dip in dR/dT . The errors bars for T_c characterize the width of the superconducting transition, with values corresponding to 20% and 80% of R_0 , where R_0 is the resistance just before the onset of superconductivity. In cases where $R(T)$ does not drop to 20% of R_0 at the lowest measured temperature, $R(T)$ is extrapolated to obtain an estimate. (b) Pressure dependence of the residual resistance R_0 and the electrical resistance change $\delta R = R(300 \text{ K}) - R_0$. R_0 for sample #2 is divided by 2, and plotted together with R_0 for sample #1. δR was only measured for sample #1. The solid lines are guides-to-the-eye.

Despite the qualitative agreement on the presence of two-dome superconductivity in the literature, directly comparing phase diagrams for RbV_3Sb_5 from this work and Ref. [24] [Fig. 6(a)], and for KV_3Sb_5 from Refs. [21, 24] [Fig. 6(b)], reveal clear differences. The differences likely originate from hydrostaticity of the experiments, which either used silicon oil as a liquid pressure medium (solid symbols, this work and Ref. [21]), or cubic boron nitride as a solid pressure medium (open symbols, Ref. [24]), with the former typically associated with better hydrostaticity. As can be seen, in the phase diagrams of both RbV_3Sb_5 and KV_3Sb_5 obtained using a liquid pressure medium, a larger pressure is required to suppress the first superconducting dome (and induce the onset of the second dome), compared to experiments using a solid pressure medium. On the other hand, superconductivity in the second dome appears more easily suppressed using a liquid medium, while it is more persistent when using a solid medium. While the origin for these systematic differences remain unclear, a key factor is the strongly anisotropic compression revealed under pressure, with the c -axis lattice parameter reduced by a staggering $\sim 20\%$ under 20 GPa in CsV_3Sb_5 [33]. Since typical studies on layered materials in a DAC applies force along the c -axis, nonideal hydrostaticity could lead to larger-than-nominal compressive pressure on the ab -plane. This may contribute to the smaller nominal pressures in experiments using a solid pressure medium, which are needed to access, for example, the dip in T_c between the two superconducting domes. These observations point to the importance of hydrostaticity for experimentally determined phase diagrams, which should be taken into consideration when comparing experimental results on AV_3Sb_5 obtained under high-pressures.

Comparing the present results on RbV_3Sb_5 with previous work on KV_3Sb_5 [21] [solid symbols in Figs. 6(a) and (b)], it can be seen that a higher pressure is required to fully suppress the first superconducting dome in RbV_3Sb_5 , consistent with the notion that a larger atomic radius corresponds to negative chemical pressure. More importantly, clear changes in the normal state transport (R_0 and δR), which can be attributed to a high-pressure phase, are

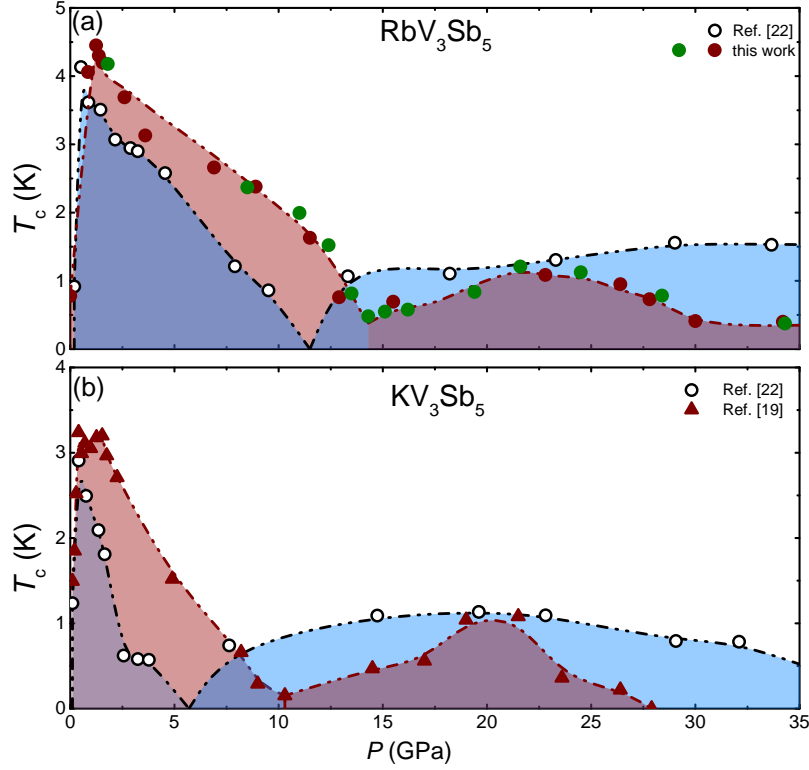


Figure 6: (a) Comparison between superconducting phase diagrams of RbV_3Sb_5 from this work and Ref. [24]. The maroon symbols are from RbV_3Sb_5 sample #1, and the green symbols are from sample #2. (b) Comparison between superconducting phase diagrams of KV_3Sb_5 from Refs. [21, 24]. T_c in this work and Ref. [21] is defined as when the resistance(resistivity) drops to $R_0/2(\rho_0/2)$, whereas it is determined from $0.9\rho_0$ in Ref. [24]. The dashed lines are guides-to-the-eye.

seen under pressures associated with the suppression of T_c in the second superconducting dome, for both RbV_3Sb_5 and KV_3Sb_5 [21]. With increasing pressure, the dR/dT anomaly near T^* first appears at the edge of the first superconducting dome, and persists across the second superconducting dome. Previous work on KV_3Sb_5 [21] also associated the resistance anomalies around T^* with the high-pressure phase and the suppression of T_c in the second superconducting dome. Examination of the published data reveals that these anomalies in KV_3Sb_5 also extend to lower pressures, suggesting that they are not unique to the high-pressure phase, similar to the present results on RbV_3Sb_5 .

It is interesting to note that for pressures associated with the second superconducting dome in CsV_3Sb_5 , Raman spectroscopy detected distinct signatures in the phonon spectrum [22], and first-principles calculations found a structural instability [32] and a reconstruction of the Fermi surface [33], suggesting that the normal state from which superconductivity emerges in the second dome of CsV_3Sb_5 is distinct from that at lower pressures, similar to the present findings for RbV_3Sb_5 . Further work is needed to understand the nature of high-pressure phases in AV_3Sb_5 , as well as clarify how they relate to the second superconducting dome.

In conclusion, we have systematically studied the electrical resistance of RbV_3Sb_5 by applying hydrostatic pressure via a liquid pressure medium, revealing the presence of two superconducting domes and distinct features in the normal state transport associated with the second dome, similar to KV_3Sb_5 . In both systems, the shape of the first superconducting dome is highly asymmetric, with maximal T_c near the border of the ambient pressure charge order. With increasing pressure, anomalies in dR/dT near $T^* \sim 220$ K appears at the edge of the first superconducting dome and persists across the second dome. The suppression of superconductivity in the second superconducting dome is associated with significant changes in the normal state transport, which can be attributed to a high-pressure phase. The commonality of a second superconducting dome at high pressures and behaviors in the normal state resistance for both RbV_3Sb_5 and KV_3Sb_5 suggests a link between these phenomena.

Acknowledgments

This work was supported by the National Key R&D Program of China (No. 2017YFA0303100, No. 2016YFA0300202), the Key R&D Program of Zhejiang Province, China (2021C01002), the National Natural Science Foundation of China (No. 11974306 and No. 12034017), and the Fundamental Research Funds for the Central Universities of China. S.D.W. and B.R.O. gratefully acknowledge support via the UC Santa Barbara NSF Quantum Foundry funded via the Q-AMASE-i program under award DMR-1906325. B.R.O. also acknowledges support from the California NanoSystems Institute through the Elings fellowship program.

* Electronic address: yusong_phys@zju.edu.cn

† Electronic address: hqyuan@zju.edu.cn

- [1] Ortiz B R, Gomes L C, Morey J R, Winiarski M, Bordelon M, Mangum J S, Oswald I W H, Rodriguez-Rivera J A, Neilson J R, Wilson S D, Ertekin E, McQueen T M and Toberer E S 2019 *Physical Review Materials* **3** URL <https://doi.org/10.1103/physrevmaterials.3.094407>
- [2] Ortiz B R, Teicher S M, Hu Y, Zuo J L, Sarte P M, Schueller E C, Abeykoon A M, Krogstad M J, Rosenkranz S, Osborn R, Seshadri R, Balents L, He J and Wilson S D 2020 *Physical Review Letters* **125** URL <https://doi.org/10.1103/physrevlett.125.247002>
- [3] Yin Q, Tu Z, Gong C, Fu Y, Yan S and Lei H 2021 *Chinese Physics Letters* **38** 037403 URL <https://doi.org/10.1088/0256-307x/38/3/037403>
- [4] Ortiz B R, Sarte P M, Kenney E M, Graf M J, Teicher S M L, Seshadri R and Wilson S D 2021 *Physical Review Materials* **5** URL <https://doi.org/10.1103/physrevmaterials.5.034801>
- [5] Wang Y, Yang S, Sivakumar P K, Ortiz B R, Teicher S M L, Wu H, Srivastava A K, Garg C, Liu D, Parkin S S P, Toberer E S, McQueen T, Wilson S D and Ali M N 2020 (*Preprint* arXiv:2012.05898)
- [6] Liang Z, Hou X, Zhang F, Ma W, Wu P, Zhang Z, Yu F, Ying J J, Jiang K, Shan L, Wang Z and Chen X H 2021 *Physical Review X* **11** URL <https://doi.org/10.1103/physrevx.11.031026>
- [7] Yang S Y, Wang Y, Ortiz B R, Liu D, Gayles J, Derunova E, Gonzalez-Hernandez R, Šmejkal L, Chen Y, Parkin S S P, Wilson S D, Toberer E S, McQueen T and Ali M N 2020 *Science Advances* **6** eabb6003 URL <https://doi.org/10.1126/sciadv.abb6003>
- [8] Yu F H, Wu T, Wang Z Y, Lei B, Zhuo W Z, Ying J J and Chen X H 2021 *Phys. Rev. B* **104**(4) L041103 URL <https://link.aps.org/doi/10.1103/PhysRevB.104.L041103>
- [9] Kenney E M, Ortiz B R, Wang C, Wilson S D and Graf M J 2021 *Journal of Physics: Condensed Matter* **33** 235801 URL <https://doi.org/10.1088/1361-648x/abe8f9>
- [10] Jiang Y X, Yin J X, Denner M M, Shumiya N, Ortiz B R, Xu G, Guguchia Z, He J, Hossain M S, Liu X, Ruff J, Kautzsch L, Zhang S S, Chang G, Belopolski I, Zhang Q, Cochran T A, Multer D, Litskevich M, Cheng Z J, Yang X P, Wang Z, Thomale R, Neupert T, Wilson S D and Hasan M Z 2021 *Nature Materials* URL <https://doi.org/10.1038/s41563-021-01034-y>
- [11] Feng X, Jiang K, Wang Z and Hu J 2021 *Science Bulletin* URL <https://doi.org/10.1016/j.scib.2021.04.043>
- [12] Setty C, Hu H, Chen L and Si Q 2021 *2105.15204* URL <https://arxiv.org/abs/2105.15204>
- [13] Lin Y P and Nandkishore R M 2021 *arXiv:2107.09050* URL <https://arxiv.org/abs/2107.09050>
- [14] Duan W, Nie Z, Luo S, Yu F, Ortiz B R, Yin L, Su H, Du F, Wang A, Chen Y, Lu X, Ying J, Wilson S D, Chen X, Song Y and Yuan H 2021 *Sci. China-Phys. Mech. Astron.* **64** 107462 URL <http://engine.scichina.com/doi/10.1007/s11433-021-1747-7>
- [15] Mu C, Yin Q, Tu Z, Gong C, Lei H, Li Z and Luo J 2021 *Chinese Physics Letters* **38** 077402 URL http://cpl.iphy.ac.cn/EN/abstract/article_105951.shtml
- [16] Xu H S, Yan Y J, Yin R, Xia W, Fang S, Chen Z, Li Y, Yang W, Guo Y and Feng D L 2021 *Phys. Rev. Lett.* **127**(18) 187004 URL <https://link.aps.org/doi/10.1103/PhysRevLett.127.187004>
- [17] Xiang Y, Li Q, Li Y, Xie W, Yang H, Wang Z, Yao Y and Wen H H 2021 *Nature Communications* **12** URL <https://doi.org/10.1038/s41467-021-27084-z>
- [18] Zhao C C, Wang L S, Xia W, Yin Q W, Ni J M, Huang Y Y, Tu C P, Tao Z C, Tu Z J, Gong C S, Lei H C, Guo Y F, Yang X F and Li S Y 2021 (*Preprint* arXiv:2102.08356)
- [19] Yu F H, Ma D H, Zhuo W Z, Liu S Q, Wen X K, Lei B, Ying J J and Chen X H 2021 *Nature Communications* **12** URL <https://doi.org/10.1038/s41467-021-23928-w>
- [20] Chen K, Wang N, Yin Q, Gu Y, Jiang K, Tu Z, Gong C, Uwatoko Y, Sun J, Lei H, Hu J and Cheng J G 2021 *Physical Review Letters* **126** URL <https://doi.org/10.1103/physrevlett.126.247001>
- [21] Du F, Luo S, Ortiz B R, Chen Y, Duan W, Zhang D, Lu X, Wilson S D, Song Y and Yuan H 2021 *Physical Review B* **103** URL <https://doi.org/10.1103/physrevb.103.1220504>
- [22] Chen X, Zhan X, Wang X, Deng J, Liu X B, Chen X, Guo J G and Chen X 2021 *Chinese Physics Letters* **38** 057402 URL http://cpl.iphy.ac.cn/EN/abstract/article_105899.shtml
- [23] Zhang Z, Chen Z, Zhou Y, Yuan Y, Wang S, Wang J, Yang H, An C, Zhang L, Zhu X, Zhou Y, Chen X, Zhou J and Yang Z 2021 *Physical Review B* **103** URL <https://doi.org/10.1103/physrevb.103.224513>

- [24] Zhu C C, Yang X F, Xia W, Yin Q W, Wang L S, Zhao C C, Dai D Z, Tu C P, Song B Q, Tao Z C, Tu Z J, Gong C S, Lei H C, Guo Y F and Li S Y 2021 (*Preprint arXiv:2104.14487*)
- [25] Yin L, Zhang D, Chen C, Ye G, Yu F, Ortiz B R, Luo S, Duan W, Su H, Ying J, Wilson S D, Chen X, Yuan H, Song Y and Lu X 2021 *Phys. Rev. B* **104**(17) 174507 URL <https://link.aps.org/doi/10.1103/PhysRevB.104.174507>
- [26] Wang N N, Chen K Y, Yin Q W, Ma Y N N, Pan B Y, Yang X, Ji X Y, Wu S L, Shan P F, Xu S X, Tu Z J, Gong C S, Liu G T, Li G, Uwatoko Y, Dong X L, Lei H C, Sun J P and Cheng J G 2021 *Phys. Rev. Research* **3**(4) 043018 URL <https://link.aps.org/doi/10.1103/PhysRevResearch.3.043018>
- [27] Wang W S, Li Z Z, Xiang Y Y and Wang Q H 2013 *Physical Review B* **87** URL <https://doi.org/10.1103/physrevb.87.115135>
- [28] Isakov S V, Wessel S, Melko R G, Sengupta K and Kim Y B 2006 *Physical Review Letters* **97** URL <https://doi.org/10.1103/physrevlett.97.147202>
- [29] Guo H M and Franz M 2009 *Physical Review B* **80** URL <https://doi.org/10.1103/physrevb.80.113102>
- [30] Kiesel M L, Platt C and Thomale R 2013 *Physical Review Letters* **110** URL <https://doi.org/10.1103/physrevlett.110.126405>
- [31] Wen J, Rüegg A, Wang C C J and Fiete G A 2010 *Physical Review B* **82** URL <https://doi.org/10.1103/physrevb.82.075125>
- [32] Zhang J F, Liu K and Lu Z Y 2021 *Phys. Rev. B* **104**(19) 195130 URL <https://link.aps.org/doi/10.1103/PhysRevB.104.195130>
- [33] Tsirlin A A, Fertey P, Ortiz B R, Klis B, Merkl V, Dressel M, Wilson S D and Uykur E 2021 *arXiv:2105.01397 (Preprint 2105.01397)*
- [34] Lee S, Collini J, Sun S X L, Mitrano M, Guo X, Eckberg C, Paglione J, Fradkin E and Abbamonte P 2021 *Physical Review Letters* **127** URL <https://doi.org/10.1103/physrevlett.127.027602>
- [35] Werthamer N R, Helfand E and Hohenberg P C 1966 *Phys. Rev.* **147**(1) 295–302 URL <https://link.aps.org/doi/10.1103/PhysRev.147.295>